ARTICLE

Forearc carbon sink reduces long–term volatile recycling into the mantle

P. H. Barry[1,25]*, J. M. de Moor[2,3,28], D. Giovannelli[4,5,6,26,28], M. Schrenk[7], D. R. Hummer[8], T. Lopez[9], C. A. Pratt[10], Y. Alpízar Segura[11], A. Battaglia[12], P. Beaudry[13], G. Bini[14], M. Cascante[2], G. d'Errico[4,15], M. di Carlo[15], D. Fattorini[15,16], K. Fullerton[17], E. Gazel[18], G. González[11], S. A. Halldórsson[19], K. Iacovino[20,27], T. Ilanko[21], J. T. Kulongoski[22], E. Manini[4], M. Martínez[2], H. Miller[7], M. Nakagawa[6], S. Ono[13], S. Patwardhan[5], C. J. Ramírez[11], F. Regoli[15,16], F. Smedile[4,5], S. Turner[23], C. Vetriani[5], M. Yücel[24], C. J. Ballentine[1], T. P. Fischer[3], D. R. Hilton[22,29] & K. G. Lloyd[17,28]

Carbon and other volatiles in the form of gases, fluids or mineral phases are transported from Earth's surface into the mantle at convergent margins, where the oceanic crust subducts beneath the continental crust. The efficiency of this transfer has profound implications for the nature and scale of geochemical heterogeneities in Earth's deep mantle and shallow crustal reservoirs, as well as Earth's oxidation state. However, the proportions of volatiles released from the forearc and backarc are not well constrained compared to fluxes from the volcanic arc front. Here we use helium and carbon isotope data from deeply sourced springs along two cross–arc transects to show that about 91 per cent of carbon released from the slab and mantle beneath the Costa Rican forearc is sequestered within the crust by calcite deposition. Around an additional three per cent is incorporated into the biomass through microbial chemolithoautotrophy, whereby microbes assimilate inorganic carbon into biomass. We estimate that between 1.2×10^8 and 1.3×10^{10} moles of carbon dioxide per year are released from the slab beneath the forearc, and thus up to about 19 per cent less carbon is being transferred into Earth's deep mantle than previously estimated.

Terrestrial carbon traverses various reservoirs on Earth from the surface to the mantle. It is subjected to a number of geological, geochemical and biological cycles, each of which operates on vastly different temporal and spatial scales. Perhaps the most important physical process linking the deep and shallow carbon cycles is subduction, which transports both oxidized and reduced forms of crustal carbon into the mantle. During subduction, volatile-rich fluids are released from the upper mantle and crustal portions of the downgoing slab. These fluids are thought to migrate through the overlying mantle wedge and crust, and are ultimately released across the forearc, volcanic arc front and backarc. However, little is known about what effect volatile fluxes through the forearc may have on the total volatile budget and estimates of recycling efficiency[1]. Much of the forearc subsurface is at low temperatures ($<100\,°C$) that are conducive to microbial life as well as shallow low-temperature water–rock interactions. Therefore, microorganisms and abiotic chemical processes may alter the speciation and isotopic composition of carbon, and thus estimated carbon budgets for convergent margins. To our knowledge, regional-scale effects of these shallow processes on volatile fluxes in the forearc have not previously been quantified.

Carbon budgets for convergent margins typically assume negligible carbon emissions from the area between the trench (that is, where the downgoing slab subducts beneath the overriding plate) and the

degassing volcanic arc front[1–3]. It is not clear whether the lack of obvious high emission sources reflects a lack of deep CO_2 input from the slab–mantle mixture, or whether secondary processes in the upper plate[4,5] mask diffuse but substantial CO_2 release.

Carbon outputs at the Central American Volcanic Arc, which have been the focus of several studies, are estimated to represent only 12% of the total subducted carbon input along the middle American trench[2,6,7], whereas global arcs typically have carbon outputs that approach their inputs, suggesting limited volatile delivery to the mantle[1]. However, recent work[8] proposed a far higher volcanic carbon flux for Central America, suggesting that this region may be more similar to other arc segments[1] than previously thought[2,6]. Our study focuses on the Nicoya Peninsula area of Costa Rica in part because it is one of the few places on Earth with easy sampling access to an on-land forearc region and thus presents an opportunity to study the fate of carbon across an entire arc. Few carbon flux estimates have been made from the forearc region of any arc, despite the fact that there is plentiful ancillary evidence for fluid venting in forearc regions, such as serpentinite diapirism in the Marianas[9] and mud volcanism at various accretionary prisms worldwide[10], as well as ample geophysical evidence of fluid upwelling in the forearc region from the downgoing slab[11]. In Costa Rica, the only available forearc data are from three submarine venting sites[3], where

[1]Department of Earth Sciences, University of Oxford, Oxford, UK. [2]Observatorio Volcanológico y Sismológico de Costa Rica (OVSICORI), Universidad Nacional, Heredia, Costa Rica. [3]Department of Earth and Planetary Sciences, University of New Mexico, Albuquerque, NM, USA. [4]Institute for Marine Biological and Biotechnological Resources, National Research Council of Italy (CNR-IRBIM), Ancona, Italy. [5]Department of Marine and Coastal Science, Rutgers University, New Brunswick, NJ, USA. [6]Earth-Life Science Institute, Tokyo Institute for Technology, Tokyo, Japan. [7]Department of Earth and Environmental Sciences, Michigan State University, East Lansing, MI, USA. [8]Department of Geology, Southern Illinois University, Carbondale, IL, USA. [9]Geophysical Institute, University of Alaska, Fairbanks, AK, USA. [10]Graduate School of Oceanography, University of Rhode Island, Kingston, RI, USA. [11]Volcanes Sin Fronteras (VSF), San Jose, Costa Rica. [12]Department of Earth and Marine Sciences, Università degli Studi di Palermo, Palermo, Italy. [13]Department of Earth, Atmospheric and Planetary Sciences, Massachusetts Institute of Technology, Cambridge, MA, USA. [14]Department of Earth Sciences, University of Florence, Florence, Italy. [15]Dipartimento di Scienze della Vita e dell'Ambiente (DISVA), Università Politecnica delle Marche (UNIVPM), Ancona, Italy. [16]CoNISMa, Consorzio Nazionale Interuniversitario Scienze del Mare, Rome, Italy. [17]Department of Microbiology, University of Tennessee, Knoxville, TN, USA. [18]Department of Earth and Atmospheric Sciences, Cornell University, Ithaca, NY, USA. [19]NordVulk, Institute of Earth Sciences, University of Iceland, Reykjavík, Iceland. [20]School of Earth and Space Exploration, Arizona State University, Tempe, AZ, USA. [21]Department of Geography, University of Sheffield, Sheffield, UK. [22]Geosciences Research Division, Scripps Institution of Oceanography, University of California, San Diego, CA, USA. [23]Department of Earth and Planetary Sciences, Washington University in St Louis, St Louis, MO, USA. [24]Institute of Marine Sciences, Middle East Technical University, Erdemli, Turkey. [25]Present address: Marine Chemistry and Geochemistry Department, Woods Hole Oceanographic Institution, Woods Hole, MA, USA. [26]Present address: Department of Biology, University of Naples Federico II, Naples, Italy. [27]Present address: Johnson Space Center, NASA, Houston, TX, USA. [28]These authors contributed equally: J. M. de Moor, D. Giovannelli, K. G. Lloyd. [29]Deceased: D. R. Hilton. *e-mail: pbarry@whoi.edu
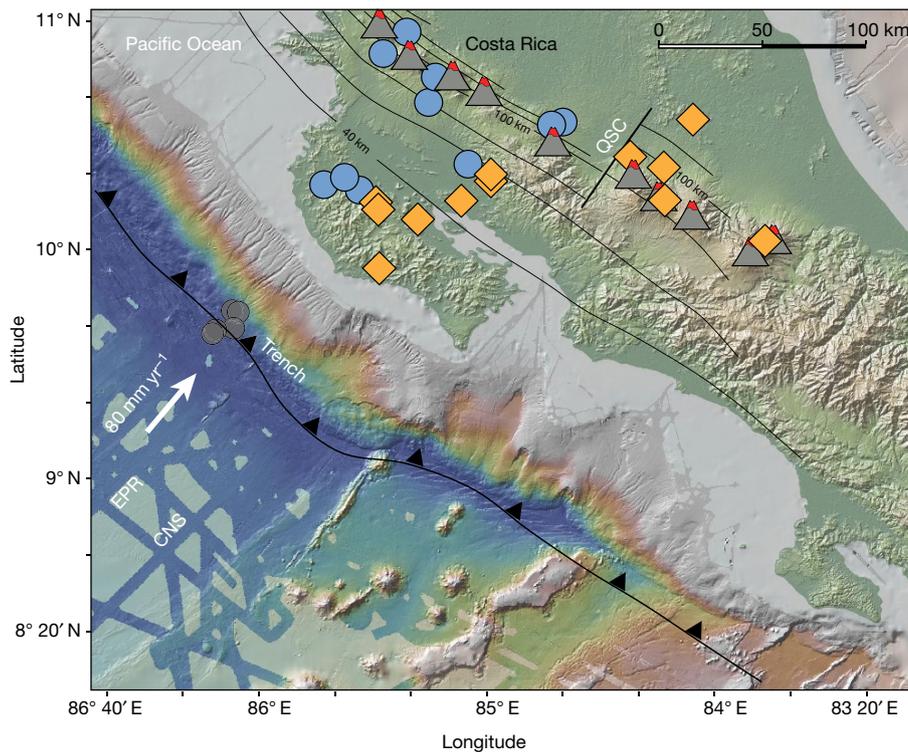
Fig. 1 | Map of the northwest coast of Costa Rica. Northern sites (blue) and central sites (orange) as well as the plate boundary between the EPR crust and the CNS crust, and the Quesada Sharp Contortion (QSC) are shown. Sample distances to trench (Supplementary Table 1) were calculated as the distance of a line segment extending from the sample location, along the angle of convergence, to the plate boundary[48]. Red-tipped triangles are volcanoes Orosí, Rincón dela Vieja, Miravalles, Tenorio, Arenal, Platanar, Poás, Barva, Turrialba, and Irazú, from North to South. The offshore trench location is shown by the black line with triangles attached, and IODP core locations are shown by grey circles. Thin lines are depth to slab in 20-km intervals[49]. Background data from GeoMapApp (http://www.geomapapp.org)[50].

the authors estimated that the carbon output from the outer forearc represents less than 1% of the carbon input at the trench. Taking into account the loss at the volcanic arc front, they proposed two explanations: either subducted carbon was largely transported into the deep mantle, or substantial quantities of carbon were lost to the forearc or backarc regions. Independently, thermodynamic models of subduction predict considerable carbon dioxide (CO_2) loss (decarbonation) from the top of the subducting slab beneath global forearc regions[12], as the slab penetrates to greater temperature and pressure conditions.

The extensive occurrence of calcite veining throughout the Costa Rican forearc[13,14] suggests that much of the CO_2 released from the slab beneath the forearc could be sequestered into the crust as calcite, in which case direct measurements of diffuse degassing in this region are not representative of the actual amount of carbon being released from the slab. Additional mechanisms for masking CO_2 gas release in the upper plate include microbial biomass production, conversion to methane (CH_4), trapping in reservoirs beneath impermeable caps, and abiotic organic matter synthesis. Calcite deposition results in a temperature-dependent isotope fractionation and may be microbially mediated[15,16] in cation-rich alkaline waters with high aqueous CO_2 concentrations. Additionally, in the absence of light for photosynthesis, microorganisms in subsurface settings instead fix CO_2 into the biomass through chemolithoautotrophy[17–19]. Both calcite deposition and chemolithoautotrophy occur mostly at temperatures below 100 °C, which are the prevalent conditions in the forearc subsurface[20]. Biologically induced carbon fixation generally results in a kinetic fractionation of carbon isotopes that preferentially removes ^{12}C from CO_2 (ref. [21]). The degree of fractionation depends on the physiology of the microorganism, as well as substrate limitations, temperature and pressure. Biological activity can also decrease the carbon isotopic composition ($\delta^{13}C$) of CO_2, by adding ^{13}C-depleted carbon through heterotrophic respiration of organic matter or methane. This process is not associated with a large carbon isotope fractionation[21] compared to pure kinetic

reactions driven solely by biological processes. In addition, abiotic hydrocarbon production from dissolved CO_2 has been demonstrated in laboratory experiments over 250 °C[22], a possible temperature regime in hotter forearc regions.

Helium and carbon results

During the 2017 field campaign we collected samples from 22 sites in northern and central Costa Rica (Fig. 1), which traversed the forearc (Nicoya Peninsula), arc and backarc regions. Springs likely to represent deeply sourced fluids (based on field data such as temperature, dissolved oxygen and salinity) were targeted, and samples were taken by inserting tubing into outflow vents to minimize fluid interaction with atmosphere and surface water. The sites were classified into two groups: the northern and central transect samples. The two groups are separated by the on-land extension of a major transition in the downgoing slab: the boundary between oceanic crust formed at the East Pacific Rise (EPR) and the Cocos Nazca Spreading centre (CNS) zone. We measured $^3He/^4He$ versus air, expressed as (R/R_A), where $R = {}^3He/{}^4He_{sample}$ and $R_A = {}^3He/{}^4He_{air} = 1.39 \times 10^{-6}$ for 17 geothermal fluid (spring water) samples and 17 free gas samples. In addition, we measured $\delta^{13}C$ versus Vienna Pee Dee Belemnite (VPDB) in dissolved inorganic carbon (DIC) in 31 geothermal fluid samples, dissolved organic carbon (DOC) in 16 fluid samples, and CO_2 in 16 free gas samples (Supplementary Table 1). Sediments surrounding the surface emanation of the springs were also sampled and total organic carbon (TOC) contents and $\delta^{13}C$ were measured. The relative abundances of He to CO_2 are also reported ($CO_2/^3He$; Extended Data Fig. 1 and Supplementary Table 1). We use the X value, which is calculated as the air-normalized $^4He/^{20}Ne$ ratio, (multiplied by the Bunsen solubility (1.23) at the assumed recharge temperature of 15 °C for fluid samples[23]), to estimate the air-corrected $^3He/^4He$ ratio (R_C) of the sample[24]. As X values are high (>5) for the majority of samples of this study (Extended Data Fig. 2), the correction factor is small and hence there is typically

little difference between measured (R/R_A) and corrected (R_C/R_A) ^{3}He/^{4}He ratios (Supplementary Table 1).

The air-corrected ^{3}He/^{4}He (R_C/R_A) values range from $0.49R_A$ to $6.79R_A$ (Supplementary Table 1), with the highest values occurring in the volcanic arc and the lowest occurring in the outer forearc. Arc values approach upper mantle values (about $8R_A$); however, they exhibit evidence for a small but discernible addition of radiogenic helium at all locations. By contrast, outer forearc and forearc values are predominantly radiogenic, with a small but distinct mantle contribution, suggesting that these fluids are an admixture of crustal fluids and deeply sourced volatiles, probably influenced by shallow water–rock interaction. He-isotope values are systematically higher (more mantle-like) in both fluids and gases close to the volcanic arc front and lower towards the trench (in the forearc; Fig. 2a), showing that slab/mantle outgassing is not limited to the volcanic arc front, and occurs throughout the entire forearc. However, free CO_2 gas (bubbling springs) was only detected within about 20 km of the arc (Fig. 2b). In the absence of gas manifestations, we examined evidence for forearc carbon processing in dissolved carbon (DC) from spring outflows.

The δ^{13}C and carbon content of DIC and DOC within spring fluids decrease systematically trenchward across the entire arc (Fig. 2b and Fig. 3). Strikingly, DIC values in northern and central Costa Rica follow distinct parallel trends (Fig. 3), which are not masked by site-dependent surface-derived organic material heterogeneities, such as vegetation, degradation of photosynthetic organic matter or surface water infiltration, indicating that the distribution of carbon in these fluids results from deep subsurface phenomena. By contrast, TOC is heavily influenced by surface detrital carbon and shows no apparent trend between concentration and δ^{13}C in samples across the two transects. DIC and DOC define Rayleigh distillation curves, with northern springs showing consistently higher δ^{13}C for both DIC and DOC at a given DIC content. The parallel trends of decreasing δ^{13}C with decreasing DIC are consistent with isothermal (about 65 °C) precipitation of isotopically heavy calcite from forearc fluids (see Methods for details), with generally higher degrees of calcite precipitation observed closer to the trench. This model is supported by water chemistry data; PhreeqC was used to show that all outer forearc samples are strongly saturated with respect to calcite and thus would be predicted to readily precipitate calcite (Supplementary Table 3). We present a model for calcite precipitation that closely fits the observed data distribution (Fig. 3), but requires a more positive δ^{13}C value of the deep total dissolved carbon (DC = DIC + DOC) source fluid (+5.0‰) released from the slab in northern Costa Rica than in central Costa Rica (+0.5‰). Volcanic gases, which are presumed to represent the primary magmatic fluid, show isotopically more negative values than DC in the calculated DIC endmember fluids, owing to the additional isotopic fractionation associated with dissolution of CO_2 gas into an aqueous fluid[25] (Fig. 3). Importantly, the modelled initial DC values thus reflect both the isotopic composition of the subduction fluids and a fractionation effect derived from CO_2 dissolution by source gases[26,27] (Fig. 3). Our data suggest that surface carbon expressions across the forearc are ultimately inherited from slab or mantle fluids, which are intricately linked to the tectonics of the region, and modified by broadly coherent shallow processes.

Origin of fluids

The observation that northern and central Costa Rica samples have markedly different source fluid compositions suggests a relationship to the character of the subducting slab. The northern EPR crust has a higher density of seamounts and is more permeable than the CNS crust[28]. The higher resulting fluid flow through sub-seafloor basalts at the EPR cools, hydrates and chemically weathers the plate[29]. Building on previous models[30], we hypothesize that the higher fluid flow from this water-rich downgoing slab flushes more carbon from the slab upward into the overriding plate at shallower depths beneath the forearc, accounting for the greater contributions of relatively ^{13}C-enriched carbonates in our northern sample set. Additionally, enhanced fluid circulation in the EPR crust probably promotes calcite
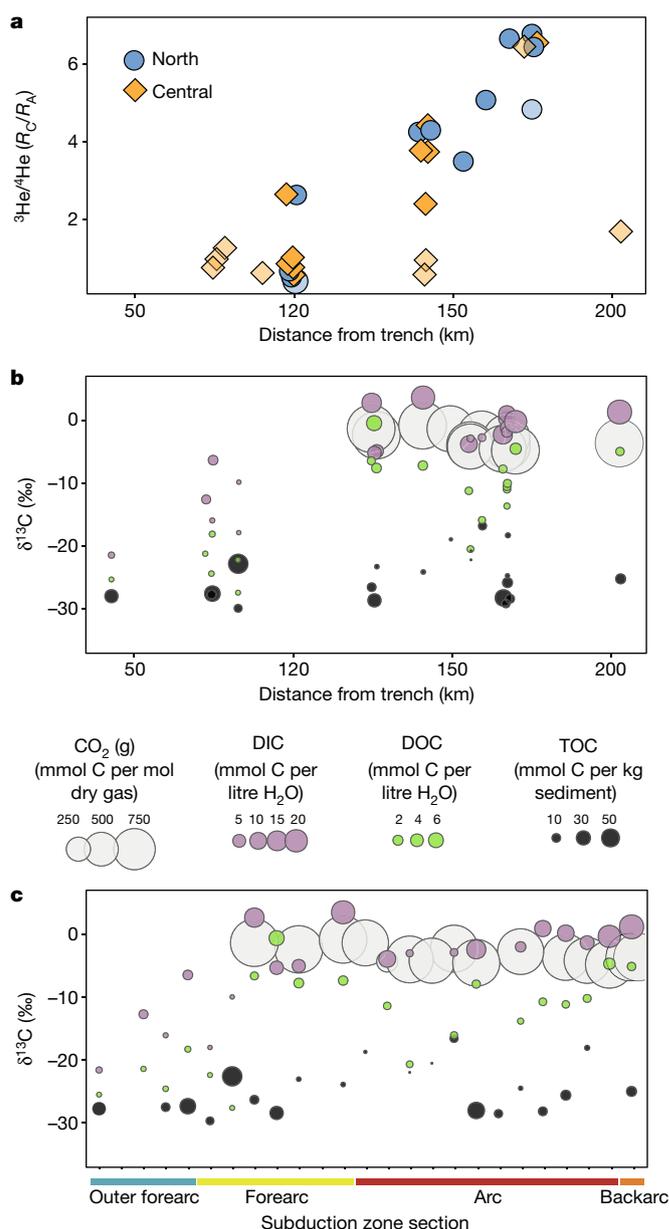

Fig. 2 | Helium and carbon isotopes across the Costa Rican convergent margin. Helium and carbon isotopic changes suggest that pervasive deep slab/mantle degassing occurs across the entire arc, even though free CO_2 gas is absent in the forearc. **a**, Helium isotopes (^{3}He/^{4}He), calculated as R_C/R_A, versus distance from trench. The lighter colours correspond to X values of less than 5. **b**, **c**, Carbon concentrations (as indicated by circle size) and δ^{13}C of CO_2 gas, DIC, DOC and TOC in sediments surrounding the surface emanation of the springs (TOC) are shown versus distance from trench (**b**) and subduction zone section (**c**) in order to show the full range in data. These 'bubble plots' show that there is a corresponding decrease in carbon concentrations and δ^{13}C values of DIC and DOC trenchward, and no change in concentrations and δ^{13}C values of TOC.

veining in the downgoing plate, potentially providing an additional source of isotopically heavy carbon[31] in northern Costa Rica. Thus, the composition of the subducting slab is expressed in surface manifestations across the forearc. Our model predicts that source fluids from northern Costa Rica are more ^{13}C-enriched than in central Costa Rica (Fig. 3). Both volcanic-arc CO_2 and dissolved forearc carbon reflect a larger carbonate contribution in northern Costa Rica, which is consistent with previous observations in the volcanic arc that show an increased carbonate signal in northern Costa Rica, which extends into Nicaragua[30,32–36].
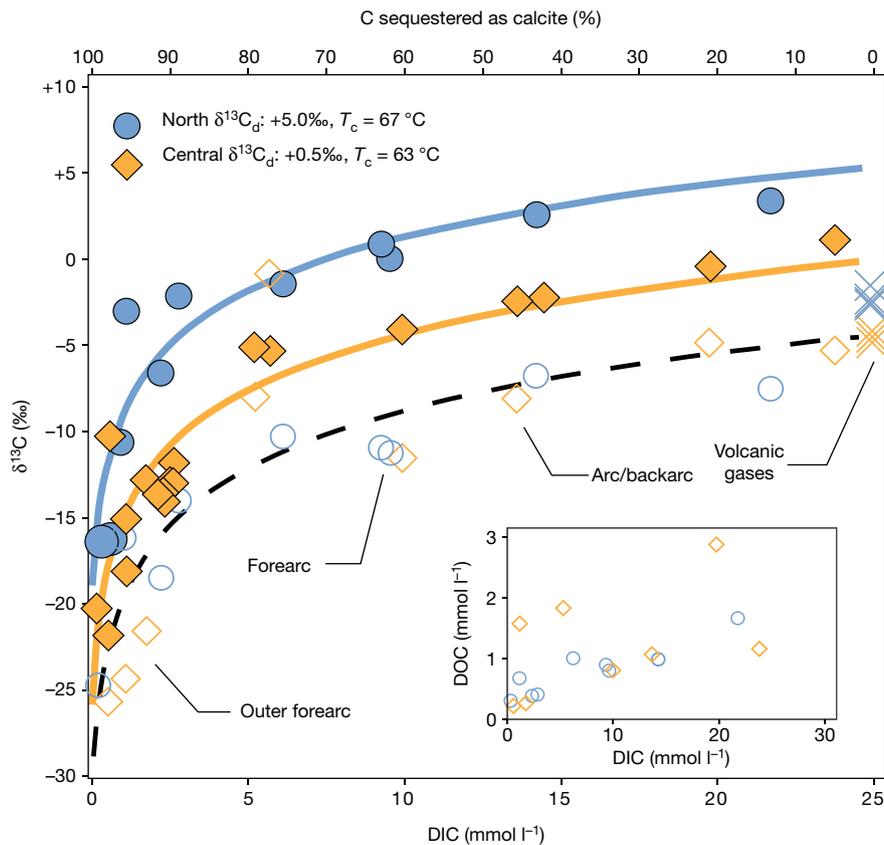
Fig. 3 | Carbon isotopes as a function of DIC concentrations for northern (blue filled symbols) and central (orange filled symbols) DIC, along with the isotope fractionation model (solid lines). DOC $\delta^{13}C$ values (open symbols) as well as DOC concentrations (inset) correlate with those of DIC, along with the DOC isotope fraction model (dashed line). For clarity, Santa Lucia (5.69 mmol DOC per litre) is not included in the inset. Crosses are free gas samples. Values for arc gases (T above boiling; plotted at 0% C sequestered as calcite) represent an endpoint of CO_2 concentration and $\delta^{13}C$, offset from DIC by the fractionation from the gas to the aqueous phase. T_c is the calculated temperature and $\delta^{13}C_d$ refers to the isotopic carbon in the dissolved phase. Seven data points were from previous expeditions, listed in Supplementary Table 1.

Importantly, the carbon isotope compositions of forearc springs can be used to calculate the fraction of carbon lost through calcite deposition (see Fig. 3 and Methods for details). Using the average $\delta^{13}C$ of the DC ($\delta^{13}C_{DC}$) of all the forearc springs for each transect (northern = −8.8‰, central = −14.3‰) we find that 88% and 89% of the total carbon released in the forearc is precipitated as calcite, respectively. Using the average $\delta^{13}C_{DC}$ of the outer forearc springs (the Nicoya Peninsula only; northern −14.4‰, central −16.5‰) yields 95% and 92% of the total carbon precipitated as calcite, for the northern and central transects, respectively. The close agreement between the calculated fractions of total carbon lost to calcite is due to the fact that the Rayleigh fractionation curves are steep at low $\delta^{13}C$ values (Fig. 3). Thus, a large range in $\delta^{13}C$ observed in the forearc corresponds to a relatively narrow range of carbon loss. We conclude that 91% ± 4% of forearc carbon is lost through calcite precipitation.

Measured DOC $\delta^{13}C$ values varied widely from −0.65‰ to −25.48‰ versus VPDB, with a mean value of −12.00‰. Like DIC, the lowest values were observed in the outer forearc and the highest values were observed in the arc, where values are highly variable (Fig. 2b, c). However, with the exception of one site in the central region (Santa Lucia), DOC carbon isotope compositions and concentrations strongly correlate with those of DIC (Fig. 3), suggesting that DOC is produced from deeply sourced fluids. Considering this, we propose a two-stage model whereby 91% ± 4% of the carbon released from the slab/mantle is consumed by calcite precipitation and the remaining DC is further fractionated by biological consumption. Our model assumes a steady-state flux of deep (slab/mantle) fluids, which imparts the carbon isotope signature of the slab into the upper plate, where carbon is partitioned into CO_2 gas, calcite, DIC and DOC. DOC is potentially a mixture of deep thermogenic DOC, deep microbial chemolithoautotrophy and shallow photosynthetic DOC. The outlier DOC sample, Santa Lucia, is probably dominated by deep thermogenic DOC, owing to the fact that it has an anomalously high DOC concentration (5.69 mmol of C per litre), $\delta^{13}C$ value (−0.65‰), and high polycyclic aromatic hydrocarbon concentrations (Supplementary Table 2), accompanied by a pronounced visible oily sheen on the surface fluids. In all other sampling sites, DOC is probably synthesized from DIC at physiologically feasible temperatures in the subsurface rather than being a mixture of exogenous sources, as its concentrations and $\delta^{13}C$ values correlate tightly with DIC.

DIC and DOC carbon isotopes are offset from each other by 10.9‰ ± 1.6‰ in the north, and by 5.8‰ ± 2.2‰ in the central region (Fig. 3); these $\Delta^{13}C_{DIC-DOC}$ are within the expected range for the reverse tricarboxylic cycle, which is a common microbial carbon fixation pathway in the subsurface[17,37]. The $\Delta^{13}C_{DIC-DOC}$ values are also consistent with isotopic fractionation of hydrocarbons synthesized abiotically from DIC at 250 °C[22]. However, calcite precipitation occurs at about 65 °C, and DOC synthesis must occur after calcite precipitation in order for DOC carbon isotope compositions to correlate with the post-precipitation DIC values. Therefore, most of the DOC appears to be derived from subsurface chemolithoautotrophy at <65 °C. This is further supported by the detection of microbial cells in all hot spring fluids except Las Hornillas. We conclude that DOC at the remaining sites is primarily synthesized from chemolithoautotrophy within the deep subsurface environment and that slab/mantle-derived carbon is used by microorganisms to build biomass. By using cell abundance values for the sampled subsurface fluids, we estimate that up to 2.8×10^9 moles of additional carbon could be locked into biomass in the Costa Rican forearc, potentially contributing substantially to the overall carbon sink.
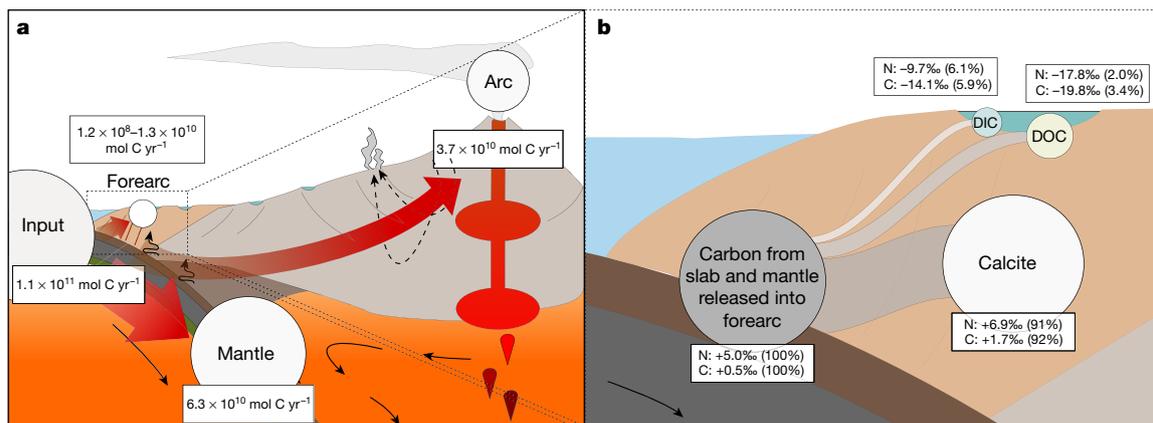
Fig. 4 | Schematic cross-section of carbon fluxes across the Costa Rican convergent margin. a, Box model showing the carbon inputs[8] in the Costa Rican forearc. Estimated inputs are from sediments, altered oceanic crust and serpentinized mantle via subduction. Estimated outputs are shown for the forearc (this study) and the arc[2,8], as well as predicted transport to the deep mantle (inputs minus outputs). **b**, Zoom view of the forearc (that is, the rectangle shown in **a**), showing endmember carbon isotopic values into the forearc following release from the slab/mantle. The model shows fluid pathways and associated fractionation as calcite forms, with approximately 91% of total carbon released in the forearc sequestered as calcite. The remaining DC is isotopically depleted and partitioned into DIC and DOC.

These findings have major implications for the global carbon mass balance of subduction zones. We calculate a CO_2 flux from the forearc (Supplementary Table 4) by combining the average DIC concentration in forearc waters of 4.24 mmol CO_2 per litre with measured flow rates, which ranged between 1 and 10 litres per second and an estimated 50–500 springs[38] throughout the forearc region. We further consider that 5–50 of these springs have a separate gas phase, with measured CO_2 fluxes of 201 mol m^{-2} d^{-1} to 655 mol m^{-2} d^{-1}, and bubbling areas that typically cover 1 m^2 to 10 m^2 (on the basis of our field observations). Using these broad criteria, the steady-state CO_2 flux is constrained to 7.1×10^6 mol yr^{-1} to 7.9×10^8 mol yr^{-1} (mean 4.0×10^8 mol yr^{-1}), which is two orders of magnitude smaller than the volcanic-arc flux of $(1.3–6.1) \times 10^{10}$ mol yr^{-1} (refs [2,8]). As argued above, carbon isotopes indicate that forearc calcite deposition and chemolithoautotrophy together remove around 94% of the total carbon inputs. This increases the flux range that we calculate to 1.2×10^8 mol yr^{-1} to 1.3×10^{10} mol yr^{-1}, which is considerably larger than the previous outer forearc estimate of 2.1×10^7 mol yr^{-1}, determined using a smaller number of submarine seeps[3]. This represents up to 36% of the total volcanic-arc flux (3.7×10^{10} mol yr^{-1}); taken as the mean of previous CO_2 flux estimates and the uncertainty value calculated from the variation $\pm 66\%$ (refs [2,8]; Fig. 4; Supplementary Table 4), which would result in a reduction of approximately 19% in the amount of total carbon transported to the deep mantle. Similarly, dissolved CH_4 concentrations and CH_4/CO_2 in sampled fluids are used to constrain the CH_4 flux from 5.1×10^3 mol yr^{-1} to 1.0×10^6 mol yr^{-1}. We show that CH_4 emissions contribute negligibly to the total forearc C budget.

Implications for evolution of Earth reservoirs

Our results suggest that less carbon is transported into Earth's mantle than previous estimates suggest[1], owing to the previously unrecognized calcite forearc carbon sink. This observation has wide-ranging implications for the volatile inventory of the mantle and the temporal evolution of Earth reservoirs, which controls the planet's redox balance[39–41]. For example, the nature (reduced versus oxidized carbon) and extent of carbon reaching the mantle is intricately linked to volatile recycling, and affects the net oxidation state of Earth's surface and deep interior. Furthermore, we propose that carbon sequestration in the forearc may be directly related to plate subduction angle, which dictates the extent of the forearc. Globally, flat subduction zones represent only about 10% of total subduction zones[42], which would indicate that approximately 2% less carbon than previously estimated is currently delivered to the deep mantle. However, such a carbon sink may have been enhanced during the late Archean eon, when oceanic crust was subducted at an anomalously low angle[43]. Notably, evidence for the so-called Archean

flat-subduction is preserved in most late Archean (3.0–2.5 billion years ago, Gyr ago) terrains, but is lacking in the early Archean (>3.3 Gyr ago). If carbon was stored overwhelmingly on continental (or island arc) margins, then continental collisions and continental arc flare-ups would be the most important regulator of atmospheric CO_2 through time. During the Proterozoic eon, subduction zones were dominated by high dip angles and smaller forearcs[44], enabling volatiles to be more efficiently transferred into the deep mantle, as the forearc carbon sink would probably be much smaller and thus transfer to the mantle would be more efficient. A more efficient transfer of reduced carbon to the mantle could then lead to enhanced accumulation of oxygen in the atmosphere over time. Thus, this work provides potential forcing mechanisms for the Great Oxygenation Event, which was most likely controlled in part by subduction efficiency and plate tectonics[45–47]. In addition, these findings also have implications for the modern atmosphere, as better constraints on the long-term volcanic carbon budget and how it may be buffered by chemical and biological processes is critical for evaluating natural and anthropogenic climate forcings.

Online content

Any methods, additional references, Nature Research reporting summaries, source data, statements of data availability and associated accession codes are available at https://doi.org/10.1038/s41586-019-1131-5.

1. Kelemen, P. B. & Manning, C. E. Reevaluating carbon fluxes in subduction zones, what goes down, mostly comes up. *Proc. Natl Acad. Sci. USA* **112**, E3997–E4006 (2015).
2. Shaw, A. M., Hilton, D. R., Fischer, T. P., Walker, J. A. & Alvarado, G. E. Contrasting He–C relationships in Nicaragua and Costa Rica: insights into C cycling through subduction zones. *Earth Planet. Sci. Lett.* **214**, 499–513 (2003).
3. Füri, E. et al. Carbon release from submarine seeps at the Costa Rica fore arc: implications for the volatile cycle at the Central America convergent margin. *Geochem. Geophys. Geosyst.* **11**, Q04S21 (2010).
4. Schwarzenbach, E. M., Früh-Green, G. L., Bernasconi, S. M., Alt, J. C. & Plas, A. Serpentinization and carbon sequestration: a study of two ancient peridotite-hosted hydrothermal systems. *Chem. Geol.* **351**, 115–133 (2013).
5. McCollom, T. M. & Seewald, J. S. Serpentinites, hydrogen, and life. *Elements* **9**, 129–134 (2013).
6. Hilton, D. R., Fischer, T. P. & Marty, B. Noble gases and volatile recycling at subduction zones. *Rev. Mineral. Geochem.* **47**, 319–370 (2002).
7. de Leeuw, G. A. M., Hilton, D. R., Fischer, T. P. & Walker, J. A. The He–CO2 isotope and relative abundance characteristics of geothermal fluids in El Salvador and Honduras: new constraints on volatile mass balance of the Central American Volcanic Arc. *Earth Planet. Sci. Lett.* **258**, 132–146 (2007).
8. de Moor, J. M. et al. A new sulfur and carbon degassing inventory for the Southern Central American Volcanic Arc: the importance of accurate time-series data sets and possible tectonic processes responsible for temporal variations in arc-scale volatile emissions. *Geochem. Geophys. Geosyst.* **18**, 4437–4468 (2017).

9. Fryer, P., Ambos, E. L. & Hussong, D. M. Origin and emplacement of Mariana forearc seamounts. *Geology* **13**, 774–777 (1985).
10. Brown, K. M. The nature and hydrogeologic significance of mud diapirs and diatremes for accretionary systems. *J. Geophys. Res. Solid Earth* **95**, 8969–8982 (1990).
11. Naif, S., Key, K., Constable, S. & Evans, R. L. Water-rich bending faults at the Middle America Trench. *Geochem. Geophys. Geosyst.* **16**, 2582–2597 (2015).
12. Gorman, P. J., Kerrick, D. M. & Connolly, J. A. D. Modeling open system metamorphic decarbonation of subducting slabs. *Geochem. Geophys. Geosyst.* **7**, Q04007 (2006).
13. Vaca, L., Alvarado, A. & Corrales, R. Calcite deposition at Miravalles geothermal field Costa Rica. *Geothermics* **18**, 305–312 (1989).
14. Corrigan, J., Mann, P. & Ingle, J. C. Jr. Forearc response to subduction of the Cocos ridge, Panama–Costa Rica. *Geol. Soc. Am. Bull.* **102**, 628–652 (1990).
15. Pacton, M. et al. Viruses as new agents of organomineralization in the geological record. *Nat. Commun.* **5**, 4298 (2014).
16. Zhu, T. & Dittrich, M. Carbonate precipitation through microbial activities in natural environment, and their potential in biotechnology: a review. *Front. Bioeng. Biotechnol.* **4**, https://doi.org/10.3389/fbioe.2016.00004 (2016).
17. Berg, I. A. Ecological aspects of the distribution of different autotrophic CO_2 fixation pathways. *Appl. Environ. Microbiol.* **77**, 1925–1936 (2011).
18. Colwell, F. S. & D'Hondt, S. Nature and extent of the deep biosphere. *Rev. Mineral. Geochem.* **75**, 547–574 (2013).
19. Emerson, J. B., Thomas, B. C., Alvarez, W. & Banfield, J. F. Metagenomic analysis of a high carbon dioxide subsurface microbial community populated by chemolithoautotrophs and bacteria and archaea from candidate phyla. *Environ. Microbiol.* **18**, 1686–1703 (2016).
20. Harris, R. N. & Wang, K. Thermal models of the middle America trench at the Nicoya Peninsula, Costa Rica. *Geophys. Res. Lett.* **29**, 2010 (2002).
21. Whiticar, M. J. Carbon and hydrogen isotope systematics of bacterial formation and oxidation of methane. *Chem. Geol.* **161**, 291–314 (1999).
22. McCollom, T. M. & Seewald, J. S. Abiotic synthesis of organic compounds in deep-sea hydrothermal environments. *Chem. Rev.* **107**, 382–401 (2007).
23. Ozima, M. & Podosek, F. A. *Noble Gas Geochemistry* (Cambridge Univ. Press, 2002).
24. Hilton, D. R. The helium and carbon isotope systematics of a continental geothermal system: results from monitoring studies at Long Valley caldera (California, U.S.A.). *Chem. Geol.* **127**, 269–295 (1996).
25. Mook, W. G., Bommerson, J. C. & Stavermann, W. H. Carbon isotope fractionation between dissolved bicarbonate and gaseous carbon dioxide. *Earth Planet. Sci. Lett.* **22**, 169–176 (1974).
26. Vogel, J. C., Grootes, P. M. & Mook, W. G. Isotopic fractionation between gaseous and dissolved carbon dioxide. *Z. Phys. A* **230**, 225–238 (1970).
27. Barry, P. H. et al. Helium and carbon isotope systematics of cold "mazuku" CO_2 vents and hydrothermal gases and fluids from Rungwe Volcanic Province, southern Tanzania. *Chem. Geol.* **339**, 141–156 (2013).
28. Audet, P. & Schwartz, S. Y. Hydrologic control of forearc strength and seismicity in the Costa Rican subduction zone. *Nat. Geosci.* **6**, 852–855 (2013).
29. Wheat, C. G. & Fisher, A. T. Massive, low-temperature hydrothermal flow from a basaltic outcrop on 23 Ma seafloor of the Cocos Plate: chemical constraints and implications. *Geochem. Geophys. Geosyst.* **9**, Q12O14 (2008).
30. Aiuppa, A. et al. Gas measurements from the Costa Rica–Nicaragua volcanic segment suggest possible along-arc variations in volcanic gas chemistry. *Earth Planet. Sci. Lett.* **407**, 134–147 (2014).
31. Alt, J. C. et al. Subsurface structure of a submarine hydrothermal system in ocean crust formed at the East Pacific Rise, ODP/IODP Site 1256. *Geochem. Geophys. Geosyst.* **11**, Q10010 (2010).
32. Carr, M. J., Feigenson, M. D. & Bennett, E. A. Incompatible element and isotopic evidence for tectonic control of source mixing and melt extraction along the Central American arc. *Contrib. Mineral. Petrol.* **105**, 369–380 (1990).
33. Leeman, W. P., Carr, M. J. & Morris, J. D. Boron geochemistry of the Central American volcanic arc: constraints on the genesis of subduction-related magmas. *Geochim. Cosmochim. Acta* **58**, 149–168 (1994).
34. Zimmer, M. M. et al. Nitrogen systematics and gas fluxes of subduction zones: insights from Costa Rica arc volatiles. *Geochem. Geophys. Geosyst.* **5**, Q05J11 (2004).
35. Hilton, D. R. et al. Monitoring of temporal and spatial variations in fumarole helium and carbon dioxide characteristics at Poás and Turrialba volcanoes, Costa Rica (2001–2009). *Geochem. J.* **44**, 431–440 (2010).
36. Lee, H. et al. Nitrogen recycling at the Costa Rican subduction zone: the role of incoming plate structure. *Sci. Rep.* **7**, 13933 (2017).
37. House, C. H., Schopf, J. W. & Stetter, K. O. Carbon isotopic fractionation by Archaeans and other thermophilic prokaryotes. *Org. Geochem.* **34**, 345–356 (2003).
38. Alvarado, G. E. & Vargas, A. G. History of discovery and exploitation of thermal water in Costa Rica. *Rev. Geol. Am. Cent.* **57**, 55–84 (2017).
39. Marty, B. & Dauphas, N. The nitrogen record of crust–mantle interaction and mantle convection from Archean to present. *Earth Planet. Sci. Lett.* **206**, 397–410 (2003).
40. Hirschmann, M. M. & Dasgupta, R. The H/C ratios of Earth's near-surface and deep reservoirs, and consequences for deep Earth volatile cycles. *Chem. Geol.* **262**, 4–16 (2009).
41. Jelen, B. I., Giovannelli, D. & Falkowski, P. G. The role of microbial electron transfer in the coevolution of the biosphere and geosphere. *Annu. Rev. Microbiol.* **70**, 45–62 (2016).
42. Li, Z. H., Xu, Z. Q. & Gerya, T. V. Flat versus steep subduction: contrasting modes for the formation and exhumation of high- to ultrahigh-pressure rocks in continental collision zones. *Earth Planet. Sci. Lett.* **301**, 65–77 (2011).
43. Smithies, R. H., Champion, D. C. & Cassidy, K. F. Formation of Earth's early Archean continental crust. *Precambr. Res.* **127**, 89–101 (2003).
44. Abbott, D., Drury, R. & Smith, W. H. F. Flat to steep transition in subduction style. *Geology* **22**, 937–940 (1994).
45. Holland, H. D. Volcanic gases, black smokers, and the great oxidation event. *Geochim. Cosmochim. Acta* **66**, 3811–3826 (2002).
46. Kump, L. R., Kasting, J. F. & Barley, M. E. Rise of atmospheric oxygen and the "upside-down" Archean mantle. *Geochem. Geophys. Geosyst.* **2**, 2000GC000114 (2001).
47. Och, L. M. & Shields-Zhou, G. A. The Neoproterozoic oxygenation event: environmental perturbations and biogeochemical cycling. *Earth Sci. Rev.* **110**, 26–57 (2012).
48. Bird, P. An updated digital model of plate boundaries. *Geochem. Geophys. Geosyst.* **4**, 1027 (2003).
49. Protti, M., Gündel, F. & McNally, K. The geometry of the Wadati–Benioff zone under southern Central America and its tectonic significance: results from a high-resolution local seismographic network. *Phys. Earth Planet. Inter.* **84**, 271–287 (1994).
50. Ryan, W. B. F. et al. Global multi-resolution topography synthesis. *Geochem. Geophys. Geosyst.* **10**, Q03014 (2009).

Author contributions P.H.B. originally conceived the idea for the project, was lead Principal Investigator (PI) on the Sloan (Deep Carbon Observatory) grant that supported the work, and prepared the first draft of the manuscript. J.M.d.M., D.G. and K.G.L. were co-PIs on the grant and contributed (and equally) to modelling these data and to the writing process. M.S. contributed to modelling and writing. D. R. Hummer, T.L. and C.A.P. were co-PIs on the Sloan grant and contributed to the writing process. Noble gas analysis was conducted in the laboratory of C.J.B. at Oxford. DIC and DOC isotope analysis were conducted by M.N. in the ELSI laboratories (Japan). Gas compositional and C isotope analyses were conducted by J.M.d.M and T.I. in the UNA laboratories (Costa Rica). T.P.F. and D. R. Hilton were the senior PIs who first brought P.H.B. and J.M.d.M. to Costa Rica as PhD students, and were instrumental in the conception of this project. In addition, a portion of the data reported in this contribution was generated from those early expeditions. All other authors (listed alphabetically) provided comments on the manuscript and either assisted in sample collection (as part of the 'Biology Meets Subduction' team or on previous expeditions) and/or analysed samples in their respective laboratories. This project was inspired by D. R. Hilton, who was a great mentor and friend.

METHODS

Sample collection and analysis. In 2017, fluid and gas samples were collected across two transects of the Costa Rican arc (Fig. 1), with pH ranging from 0.9 to 10.0 and temperatures in the range 23–89 °C. Fluid and gas samples were collected in evacuated glass flasks and copper (Cu) tubes using standard collection procedures[51], whereby precautions were taken to minimize any possible air contamination[27]. Gas and fluid samples ($n = 24$) from 2017 are accompanied by additional ($n = 17$) samples collected during reconnaissance field campaigns in 2008, 2010 and 2012. He and C isotope data from the initial reconnaissance field campaigns were produced in the Fluids and Volatiles Laboratory at Scripps Institution of Oceanography (SIO), whereas data from 2017 are from the University of Oxford (the He isotopes) and the Tokyo Institute for Technology (the C isotopes).

All samples were collected during the dry season in an effort to minimize seasonal effects (Supplementary Table 1). Considering this, the data from the various laboratories are in good agreement. For example, fluids were collected at the Sabana Grande site in 2008, 2010 and again in 2017; C isotope values of −12.69‰ (2017; Japan) agree well with −12.75‰ (2008; SIO), −12.79‰ (2008; SIO) and −13.43‰ (2012; SIO). He-isotope values for this site were $2.66 \pm 0.13 \, R_A$ (2017; Oxford), $0.60 \pm 0.03 \, R_A$ (2008; SIO) and $1.04 \pm 0.11 \, R_A$ (2012; SIO), all indicating an admixture of radiogenic and mantle derived gases. Notably, there is not thought to be a discernible cosmogenic component in subduction-related fluids, as ^{3}He outputs greatly exceed input parameters[6]. Also, much too little interplanetary dust is available to sustain the flux required[52]. When considering the reproducibility of He isotope measurements, it is essential to consider the amount of air contamination in a given sample, which is estimated using the relative amount of He and Ne, expressed as the X value (^{4}He/^{20}Ne normalized to air). At Sabana Grande, the most pristine sample (that is, with the highest X value) yielded the highest He isotope value of $2.66 \, R_A$ (Extended Data Fig. 2). Helium isotopes were also measured in samples collected at the Pueblo Antiguo site in 2010 (SIO), 2012 (SIO) and 2017 (Oxford), and in the two samples with high X values (>5), the He isotopes measured at different laboratories are within analytical error (at the University of Oxford in 2017, $4.34 \pm 0.22 \, R_A$ and at SIO in 2010, $4.51 \pm 0.11 \, R_A$).

Gas and water samples from the 2008, 2010 and 2012 campaigns were analysed at SIO for helium and carbon isotopes using instrumentation and protocols described previously[2,7,53]. All samples were extracted on a dedicated preparation line with a fraction of the non-condensable gas (containing He and Ne) captured in a 1720-glass breakseal. All CO_2 was condensed into a Pyrex breakseal following separation from water vapour, non-inert gases (N_2, CO and CH_4) and heavy noble gases (Ar, Kr and Xe).

Helium and neon analyses were carried out on a MAP-215 noble gas mass spectrometer at SIO. First, the gas was released from the breakseal and prepared for analysis using a series of traps, held at liquid nitrogen temperature, and active-gas getters. Helium was separated from neon using a helium-cooled refrigeration stage interfaced to a trap lined with activated charcoal. All sample ^{3}He/^{4}He ratios were normalized to standard aliquots of air processed and analysed under identical conditions.

Carbon dioxide was purified at SIO on a dedicated line using a variable temperature trap designed to separate CO_2 from sulfur-bearing species. Following cleanup, the amount of CO_2 was measured using a capacitance gauge manometer in a calibrated volume, before freezing an aliquot of the CO_2 in a Pyrex breakseal. For isotope analysis, the CO_2 aliquot was inlet into a Thermo-Finnigan Delta XP^{Plus} isotope ratio mass spectrometer. Carbon isotopes on gas samples from the 2017 campaign were analysed at Universidad Nacional on a Picarro G2201-I by acidification of NaOH solutions extracted from Giggenbach bottle samples. $\delta^{13}C_{VPDB}$ values were calibrated against a set of eight standards with values ranging from +2.42‰ to −37.21‰, including internationally accepted standards NBS19 and Carrara Marble. Reported $\delta^{13}C$ values have uncertainties of <0.1‰ based on repeat analyses of standards and samples.

Noble gas analysis was also conducted in the Noble Laboratory at the University of Oxford (the 2017 samples), using a dual mass spectrometer setup interfaced to a dedicated extraction and purification system[54]. Gases were collected in Cu tubes, and then transferred to the extraction and purification line where reactive gases were removed by exposing gases to a titanium sponge held at 950 °C. The titanium sponge was cooled for 15 min to room temperature (20 °C) before gases were expanded to a dual hot (SAES GP-50) and cold (SAES NP-10) getter system, held at 250 °C and room temperature, respectively. A small aliquot of gases was segregated for preliminary analysis on a Hiden Analytical HAL-200 quadrupole mass spectrometer. All noble gases were then concentrated using a series of cryogenic traps; heavy noble gases (Ar, Kr and Xe) were frozen down at 15 K on an all stainless steel finger (a stem of the vacuum line) and the He and Ne were frozen down at 19 K on a cold finger filled with charcoal. The temperature on the charcoal finger was then raised to 34 K to release only He, which was inlet into a Helix SFT mass spectrometer. Following He analysis, the temperature on the charcoal

cryogenic trap was raised to 90 K to release Ne, which was inlet into an ARGUS VI mass spectrometer.

Water samples for carbon isotope analysis (2017 samples) of DIC and DOC were collected by 50-ml syringes and filtered through a 0.22 μm filter (DISMIC–25AS; Advantec Toyo Kaisha) and directly injected into a pre-vacuumed 50-ml serum bottle sealed with butyl rubber septa and an aluminium crimp. DIC concentrations and their $\delta^{13}C$ values were measured using CO_2 in the headspace of glass vials after a 1-h reaction with injected 0.5-ml H_3PO_4. DOC were also measured from CO_2 in the headspace after the reaction of carbonate-free residue with 0.2 g sodium persulfate. The amount of CO_2 and the isotopic values were measured using a Agilent 6890N gas chromatograph attached to a Thermo-Finnigan Delta XP^{Plus}. Two international standards ($\delta^{13}C = −13.90$‰ and 2.52‰) were used for standardization, and the standard deviations were obtained from more than three measurements.

The sediments surrounding the surface emanations of the springs were collected for measuring TOC content and carbon isotopic compositions. The sediment samples were kept at 4 °C until they were transported to the laboratory. Glass vial samples were then stored at −80 °C until further treatment. First, the sediment samples were freeze-dried and then crushed into fine grains using a mortar to remove large leaves and roots. 50–100 mg of sediment samples were weighed and reacted with 1 M HCl solution until effervescence stopped, followed by a rinse with distilled water until the pH neutralized. The TOC sediment samples were analysed using an elemental analyser (EA-1110; Thermo Fisher Scientific) coupled to a Thermo Fisher Scientific MAT 252 isotope ratio mass spectrometer.

Samples for cell counts were taken in 2017 as close to the source spring as possible, usually in an outflow from a rock outcrop or a small surface pool that was rapidly being refilled by the source. We placed 1 ml of fluids into a 2-ml plastic tube with a rubber O-ring screwcap (to prevent evaporation) containing 500 μl of 3% paraformaldehyde solution in phosphate-buffered saline. Cell count samples fixed with 3% paraformaldehyde in the field were kept at room temperature during return to the University of Tennessee and were weighed upon arrival at the laboratory. Cell counts were determined on a Guava Easy Cyte 6HT-2L (Millipore) flow cytometer. Triplicate aliquots of each sample (200 μl) were stained with $5 \times$ SybrGreen before analysis. We estimated contributions of cell biomass with total cell counts, and average carbon content of subsurface microbes[55], by multiplying the average number of cells in our fluid samples by the volume of hosting rocks (from the trench to the arc, assuming a logarithmic increase of the isotherms moving towards the arc) up to depths of 2 km, and using an average rock porosity (to obtain possible fluid amounts)[56], and found that they did represent a very large carbon reservoir.

Aliphatic hydrocarbons (C10-C40) and polycyclic aromatic hydrocarbons were analysed using conventional procedures based on gas chromatography with a flame ionization detector and high-pressure liquid chromatography (HPLC) with diode array and fluorimetric detection[57]. In brief, aliphatic hydrocarbons (C10 to C40) were extracted with hexane:acetone (2:1) in a microwave (110 °C for 25 min, 800 W) (Mars CEM, CEM Corporation). After centrifugation at 3,000g for 10 min, the supernatants were purified with solid-phase extraction (Phenomenex Strata-X, 500 mg × 6 ml plus Phenomenex Strata-FL, 1,000 mg × 6 ml) and then concentrated using a SpeedVac (RC1009; grade n-hexane and analysed with a PerkinElmer gas chromatograph) equipped with an Elite-5 capillary column (30 mm length × 0.32 mm inner diameter × 0.25 μm film thickness) and a flame ionization detector. For quantitative determination, the system was calibrated with an unsaturated pair n-alkane standard mixture according to ENISO 9377-3 (Fluka 68281). For the analysis of polycyclic aromatic hydrocarbons, sediment samples were extracted using 0.5 M potassium hydroxide in methanol with microwave at 55 °C for 20 min (800 W) (CEM, Mars System). After centrifugation at 3,000g for 10 min, the methanol extracts were concentrated using a SpeedVac and purified with solid-phase extraction (Octadecyl C18, 500 mg × 6 ml, Bakerbond). A final volume of 1 ml was recovered with pure, analytical HPLC gradient grade acetonitrile; HPLC analyses were carried out in a water-acetonitrile gradient by fluorimetric and diode array detection. The polycyclic aromatic hydrocarbons were identified according to the retention times of an appropriate pure standard solution (EPA 610 Polynuclear Aromatic Hydrocarbons Mix), and classified as low molecular weight (naphthalene, acenaphthylene, 1-methyl naphthalene, 2-methyl naphthalene, acenaphthene, fluorene, phenanthrene, anthracene) or high molecular weight (fluoranthene, pyrene, benzo[a]anthracene, chrysene, 7,12-dimethyl-benzo[a]anthracene, benzo[b]fluoranthene, benzo[k]fluoranthene, benzo[a]pyrene, dibenzo[a,h]anthracene, benzo[g,h,i]perylene, indeno[1,2,3-cd]pyrene), where the letters in parentheses refer to the location of the fusion between the two molecules. Accuracy and precision were checked by analysing both pure standard solutions and reference materials (NIST 1944) and the obtained concentrations were always within the 95% confidence intervals of the certified values. Aliquots of all the samples were dried in an oven at 60 °C for at least 8 h, to obtain a constant weight, in order to quantify the interstitial water content, allowing all the analysed chemicals to be expressed as a function of the dry weight of the sediments.

Isotope fractionation modelling. He–C studies in volcanic arc settings[2,58–61] have coupled helium and carbon isotopes to distinguish carbon from different provenances using a three-component mixing model (Extended Data Fig. 1). In such acidic settings, volcanic activity has been suggested[62–65] to release previously sequestered CO_2, which mixes with slab/mantle carbon and results in the characteristic signatures. Samples from this study were collected from a range of lithologies from ophiolites in Nicoya[66–71] to andesitic and basaltic volcanic rocks in the arc and forearc. The volcanic front in Costa Rica developed on the western edge of the Caribbean Plateau, an oceanic plate basement without any pre-existing continental or arc material[72–74]. The Santa Elena ophiolite is part of a series of exotic, arc-related terrenes that form the basement of the volcanic front in southern Nicaragua and it does not extend south of the Hess Escarpment–Santa Elena suture[75,76]. However, these carbon isotope data are consistent with a model that requires a homogenous C isotope input flux. This indicates that degassing of the downgoing slab/mantle drives the ^{13}C-isotope inputs, rather than the overriding crust, but in some cases, this signal is subsequently obfuscated by low-temperature precipitation of isotopically heavy calcite, which effectively fractionates the carbon isotopes. Here we provide additional details on the fractionation modelling used to construct the calcite fractionation curves in Fig. 3.

In summary, carbon is released from the slab/mantle and reacts with shallow groundwater forming an initial pool of DC. An isotopic fractionation factor between DC and calcite (see details below) is calculated on the basis of the best fit to the observed data by varying the temperature iteratively. The starting $\delta^{13}C$ of DC is determined to be different from the northern (5.0‰) and central (0.5‰) transect, presumably controlled by different slab inputs. Notably, the presumed slab inputs are consistent with positive isotope values measured in carbonate sediments off the coast of Nicoya[77]. Starting $\delta^{13}C$ input conditions are assumed to be the same for the forearc, backarc and arc. As the Rayleigh fractionation progresses, calcite is precipitated and the isotope composition of residual DC reflects open system (Rayleigh) fractionation processes. Rayleigh distillation curves were iteratively fitted to the data using:

$$\delta^{13}C_{DC,f} \cong (\delta^{13}C_{DC,i} + 1,000)(F^{\alpha_{DC-calcite}-1}) - 1,000 \qquad (1)$$

after ref. [78], where F is the fraction of DC remaining in the fluid, $\delta^{13}C_{DC,f}$ is the carbon isotope composition of DC at F, $\delta^{13}C_{DC,i}$ is the initial isotope composition of the DC, and $\alpha_{DC-calcite}$ is the fractionation factor between DC and calcite at a given temperature. The fractionation factor between DC and calcite was calculated from ref. [79]:

$$1,000 \times \ln\alpha_{DC-calcite}$$
$$= -8.91 \times 10^8 T^{-3} + 8.557 \times 10^6 T^{-2} - 1.881 \times 10^4 T^{-1} + 8.27 \qquad (2)$$

where T is the temperature in Kelvin.

Model curves were fitted to the data from each transect by iteratively varying the values of $\delta^{13}C_{DC,i}$ and the temperature of calcite formation. Best-fit results were obtained with $\delta^{13}C_{DC,i} = +5.0$‰ and $T = 67\,°C$ (correlation coefficient $R^2 = 0.91$) for the northern transect and $\delta^{13}C_{DC,i} = +0.5$‰ and $T = 63\,°C$ ($R^2 = 0.86$) for the central transect.

Total DC values used in the model are calculated from the sum of the measured DIC and DOC concentrations (Supplementary Table 4), and $\delta^{13}C_{DC}$ is the average of $\delta^{13}C_{DIC}$ and $\delta^{13}C_{DOC}$, weighted by their respective DIC and DOC concentrations. DIC dominates the total DC contents, typically accounting for about 80% of DC on a sample by sample basis. DOC data are not available for 12 of our 30 samples, as several samples were collected on previous reconnaissance field campaigns. However, the strong correlation between DC and DIC (Extended Data Fig. 3) allows us to confidently predict the DC concentration and the $\delta^{13}C_{DC}$ values of the samples for which DOC is not available. The predicted DC and $\delta^{13}C_{DC}$ are thus used for the 12 samples for which DOC data are not available in Fig. 3. The slope of the linear regressions in Extended Data Fig. 2a, c is used to calculate the fraction of DOC in the northern and central transects (5.4% and 4.7%, respectively).

Carbon budget calculations. The carbon isotope fractionation model allows calculation of the fraction of carbon in various forearc reservoirs. Based on the average $\delta^{13}C_{DC}$ values at the forearc sites (here defined as located at <155 km from the trench), the fraction F of carbon remaining in the fluid can be calculated (expressed as the percentage of carbon sequestered as calcite in Fig. 3, which is equal to $100(1 - F)$). The average $\delta^{13}C_{DC}$ values at forearc sites are further used to calculate the total DC concentration in mmol per litre based on the Rayleigh curves. Because the curves are steep at low F values, the $\delta^{13}C_{DC}$ values represent a more robust and sensitive parameter than the DC concentrations, which are more susceptible to dilution and analytical uncertainty at low concentrations. The average DIC concentration for forearc fluid is then calculated from DC concentrations from the relationship between DC and DIC expressed in Extended Data Fig. 2a, c. In this model, DOC is then the residual carbon once DIC and calcite

concentrations are accounted for. The results of these calculations indicate that 91.3% of the total forearc carbon is sequestered as calcite, 6.0% is released at the surface as DIC, and 2.7% is consumed by microbiological processes to form DOC.

Our flux estimates for the Costa Rican forearc (see main text) show that between 7.1×10^6 and 7.9×10^8 mol yr^{-1} of CO_2 are released to the surface by spring outflow as DIC and CO_2 gas. Based on the above-described model, we argue that this represents the residual carbon left over after pervasive calcite deposition. The total flux (that is, subducted slab and mantle fluid) through the forearc, including both calcite deposition and microbial consumption, ranges from 1.2×10^8 to 1.3×10^{10} mol yr^{-1} (Fig. 4).

Previous mass balance calculations. To put our forearc flux estimates into context, we must consider previous flux estimates, which to date, have focused mostly on high-temperature regions[11–13], where there is a distinct point source for carbon emissions. However, little work has been conducted in the forearc of Costa Rica[3] even though thermodynamic modelling of the Costa Rican convergent margin predicts efficient CO_2 release from the top of the subducting slab beneath forearcs, at depths of 65–80 km (ref. [12]).

Past budget approaches[59] coupled He and C isotopes to tease apart C sourced from different provenances using a three-component mixing model (Extended Data Fig. 1). Subducted slab carbon is presumed to derive from carbonate rocks and have a value of about zero VPDB, mantle values are assumed to be approximately –6.5 ± 2.0‰ and isotopically low carbon isotope values are attributed to contributions from organic sediments (–30‰). Here we argue that in the forearc environment these values do not result from mixing, but instead from low-temperature calcite precipitation and biological consumption.

Arc fluxes are typically only measured along a relatively narrow transect source: the volcanic arc front. By contrast, springs occur over a large stretch of the forearc, so this is a much larger area to integrate. Quantitative assessment of gas fluxes from the forearc, backarc, fault-related sites, hydrothermal volcanic systems (for example, Tenorio, Miravalles, Irazú and Rincón de la Vieja flank sites) and concurrent diffuse degassing are lacking. Here we place better constraints on forearc fluxes, which complement recent constraints on magmatic C fluxes[8]. We estimate a flux of between 1.2×10^8 and 1.3×10^{10} mol yr^{-1} of CO_2, which represents as much as 36% of the total arc flux., and could reduce the amount transferred into the deep mantle by up to 19%.

Previous studies have used helium and carbon isotopes (^{3}He/^{4}He, δ^{13}C) and relative abundances ratios (CO_2/^{3}He) of fumarole sites at arc settings. Two approaches were taken in these areas in order to determine CO_2 fluxes: (1) combining measured CO_2/^{3}He data with known ^{3}He fluxes and (2) to combine measured CO_2/SO_2 data with known SO_2 fluxes. Previous work was conducted throughout Costa Rica[3,6,8], El Salvador, Honduras[7] and Nicaragua[2].

In typical subduction zones, the vast majority of carbon is thought to be recycled back into the lithosphere, hydrosphere and atmosphere[1], and what remains is transported into the deep mantle. By contrast, mass balance considerations from the Costa Rican convergent margin suggest the majority of subducted C (more than 85%) is ultimately transferred into the deep mantle[2,3,6]. Importantly, this estimation assumes that the forearc and backarc fluxes are negligible, which we have shown in this work to be untrue.

Previous work[6] estimated the subducting CO_2 input flux for the 310-km-long Costa Rican arc to be 8.2×10^{10} mol yr^{-1} (ref. [6]), assuming '1% organic CO_2' in sediments based on data from a single IODP site (number 1039) and a 'global average' altered crustal composition of 0.2% CO_2, extrapolated over the entire slab thickness. Published carbon degassing (output) flux estimates vary between 1.2×10^{10} mol yr^{-1} to 1.5×10^{10} mol yr^{-1}, with an average value of 1.26×10^{10} mol yr^{-1}. Importantly, these estimates are determined to be >90% sediment-derived and marine-carbonate-derived, based on C-isotope data[2]. However, more recent studies[8,62,80] use a more complete assessment of volcanic degassing from the arc to show that the current volcanic CO_2 flux from Costa Rica is much higher (6.10×10^{10} mol yr^{-1}). The 2017 study[8] is based on new data for 11 volcanoes in Costa Rica and Nicaragua showing that the CO_2 flux from the arc is underestimated in previous studies. Their findings suggest that the Central American subduction margin may be more similar to other arc segments[1] than previously thought[2,6]. The 2017 findings[8] suggest the 2014–2015 CO_2 flux from the Costa Rican arc is an order of magnitude greater than previous estimates[2,6]. However, the Costa Rican–Nicaraguan margin has displayed an increase in arc-wide volcanic activity in recent years[8]. Thus, arc systems probably show considerable variation in gas output over time. If the older estimates[2,6] of CO_2 flux are taken to be more representative of the time-integrated CO_2 flux, then there is still a large missing flux in the forearc or arc. In Fig. 4 we take the average value from refs [2,8] to determine an average CO_2 flux of 3.7×10^{10} mol yr^{-1} ± 66%.

Geologic background. The Central American subduction zone is characterized by rapid (70–90 mm yr^{-1}) convergence of young (15–25 million years old) oceanic lithosphere[81–83], whereas the downgoing Cocos plate is composed of a thin sedimentary layer (~428 m). The upper section of the column (177 m)

consists of Quaternary to upper Miocene hemipelagic diatomaceous mud and middle Miocene brown abyssal clay and the lower section consists of middle–lower Miocene chalky carbonate ooze and manganiferous chalk and chert[84,85]. The composition of subducted sediments and carboniferous material is microbiologically altered, owing to the fact that anaerobic respiration and fermentation determine sediment redox conditions, alkalinity and carbon isotope pools[86,87]. The entire column of incoming sediments underthrusts the toe of the Caribbean Plate. However, the absence of substantial off-scraping or sediment accretion suggests that the Costa Rican convergent margin is either non-accretionary, or underplated further landward[80,88]. Under-thrusting leads to rapid compaction of the upper hemipelagic sediments and dewatering of pore fluids within the first few kilometres of subduction[89], resulting in the release of carbon dioxide and methane at relatively shallow depths into the overlying forearc[3]. Fluids released during dehydration reactions ascend through the overriding plate along deep-penetrating faults, producing numerous fluid venting sites in the forearc of Costa Rica[90]. A considerable portion of the forearc is subaerial (the Nicoya and Osa peninsulas), providing unique sampling opportunities not found at the majority of arc systems. In addition to mechanically induced shallow dewatering near the toe of the overriding plate, deeply sourced (that is, abiotic) fluids are released by mineral dehydration reactions and phase transformations at depths of approximately 10–15 km (between 60–140 °C)[89,91], which are at pressure and temperature ranges that are within the range of theoretically habitable environments for microorganisms[92,93]. Volcanoes in Costa Rica form a part of the southern segment of the Central American Volcanic Arc. The volcanic arc in Costa Rica extends from the north to the centre of Costa Rica, immediately to the east of the Nicoya Peninsula. We collected samples for this study in the forearc, arc and backarc of this region.

Microbiological background. ^{13}C-depleted carbon dioxide in fluids released in the submarine portion of the outer forearc indicate a $\delta^{13}C$ depleted source and may imply biological production through anaerobic respiration of sulfate, which is an abundant oxidant in seawater[3]. The level of ^{13}C-depletion can be moderate ($-10‰$ to $-15‰$), suggesting electron donors from organic matter, or extreme ($-60‰$ to $-70‰$), suggesting electron donors from methane. Methanotrophy can occur anaerobically through sulfate reduction[94], or aerobically when oxygenated seawater mixes with methane-rich fluids[95]. The methane itself may be methanogenic products mobilized from the >12 km source fluids[96], or shallower methanogenesis[97], but this has yet to be resolved with isotopic analysis.

Methane in the subaerial section of the margin has been found to have a large biogenic component, with $\delta^{13}C$ of $-35‰$ to $-45‰$, and presence of methanogenic archaea[98,99]. However, no large-scale survey of the effects of microbiology on degassing across a convergent margin has been performed. The few microbiological studies that have been conducted in convergent margins have focused on a single site at a time, preventing any regional-scale exploration of how microbes interact with these deep geological processes.

Data availability
All raw data needed to make the plots are available in Supplementary Tables 1 and 2 as well as in the Source Data file provided. All data are archived through EarthChem (https://doi.org/10.1594/IEDA/111271 at http://get.iedadata.org/doi/111271).

Code availability
The freely distributed software PhreeqC (United States Geological Survey) was used to calculate geochemical solubilities, and is available for download at https://www.usgs.gov/software/phreeqc-version-3.

51. Giggenbach, W. F. & Goguel, R. L. *Methods for the Collection and Analysis of Geothermal and Volcanic Water and Gas Samples. Report CD* 2387 53 (Department of Scientific and Industrial Research (Chemistry Division), 1989).
52. Trull, T. Influx and age constraints on the recycled cosmic dust explanation for high $^3He/^4He$ ratios at hotspot volcanos. *Noble Gas Geochem. Cosmochem.* 77–88 (1994).
53. Kulongoski, J. T. & Hilton, D. R. A quadrupole-based mass spectrometric system for the determination of noble gas abundances in fluids. *Geochem. Geophys. Geosyst.* **3**, 1–10 (2002).
54. Barry, P. H. et al. Noble gases solubility models of hydrocarbon charge mechanism in the Sleipner Vest gas field. *Geochim. Cosmochim. Acta* **194**, 291–309 (2016).
55. Braun, S. et al. Cellular content of biomolecules in sub-seafloor microbial communities. *Geochim. Cosmochim. Acta* **188**, 330–351 (2016).
56. Giovannelli, D. et al. Diversity and distribution of prokaryotes within a shallow-water pockmark field. *Front. Microbiol.* https://doi.org/10.3389/fmicb.2016.00941 (2016).
57. McMahon, S. & Parnell, J. Weighing the deep continental biosphere. *FEMS Microbiol. Ecol.* **87**, 113–120 (2014).
58. Sano, Y. & Marty, B. Origin of carbon in fumarolic gas from island arcs. *Chem. Geol.* **119**, 265–274 (1995).
59. Snyder, G., Poreda, R., Hunt, A. & Fehn, U. Regional variations in volatile composition: isotopic evidence for carbonate recycling in the Central American volcanic arc. *Geochem. Geophys. Geosyst.* **2**, 1057 (2001).
60. Snyder, G., Poreda, R., Fehn, U., & Hunt, A. The geothermal fields of Central America: influence of the subduction process on its volatile composition. *Geol. Mag. Central Am.* **30**, 137–148 (2004).
61. Wehrmann, H., Hoernle, K., Portnyagin, M., Wiedenbeck, M. & Heydolph, K. Volcanic CO_2 output at the Central American subduction zone inferred from melt inclusions in olivine crystals from mafic tephras. *Geochem. Geophys. Geosyst.* **12**, Q06003 (2011).
62. de Moor, J. M. et al. Turmoil at Turrialba Volcano (Costa Rica): degassing and eruptive processes inferred from high-frequency gas monitoring. *J. Geophys. Res. Solid Earth* **121**, 5761–5775 (2016).
63. Dawson, P., Chouet, B. & Pitt, A. Tomographic image of a seismically active volcano: Mammoth Mountain, California. *J. Geophys. Res. Solid Earth* **121**, 114–133 (2016).
64. Mason, E., Edmonds, M. & Turchyn, A. V. Remobilization of crustal carbon may dominate volcanic arc emissions. *Science* **357**, 290–294 (2017).
65. Chiodini, G., Pappalardo, L., Aiuppa, A. & Caliro, S. The geological CO_2 degassing history of a long-lived caldera. *Geology* **43**, 767–770 (2015).
66. Berrangé, J. P. & Thorpe, R. S. The geology, geochemistry and emplacement of the Cretaceous—Tertiary ophiolitic Nicoya Complex of the Osa Peninsula, southern Costa Rica. *Tectonophysics* **147**, 193–220 (1988).
67. Giggenbach, W. F. Relative importance of thermodynamic and kinetic processes in governing the chemical and isotopic composition of carbon gases in high-heatflow sedimentary basins. *Geochim. Cosmochim. Acta* **61**, 3763–3785 (1997).
68. Kuijpers, E. P. The geologic history of the Nicoya Ophiolite Complex, Costa Rica, and its geotectonic significance. *Tectonophysics* **68**, 233–255 (1980).
69. Schwarzenbach, E. M. et al. Sources and cycling of carbon in continental, serpentinite-hosted alkaline springs in the Voltri Massif, Italy. *Lithos* **177**, 226–244 (2013).
70. Torgersen, T. Terrestrial helium degassing fluxes and the atmospheric helium budget: implications with respect to the degassing processes of continental crust. *Chem. Geol. Isotope Geosci. Sect.* **79**, 1–14 (1989).
71. Walther, C. H. E., Flueh, E. R., Ranero, C. R., Von Huene, R. & Strauch, W. Crustal structure across the Pacific margin of Nicaragua: evidence for ophiolitic basement and a shallow mantle sliver. *Geophys. J. Int.* **141**, 759–777 (2000).
72. Gazel, E., Denyer, P., & Baumgartner, P. O. Magmatic and geotectonic significance of Santa Elena peninsula, Costa Rica. *Geol. Acta* **4**, 0193-202 (2006).
73. Gazel, E. et al. Plume–subduction interaction in southern Central America: mantle upwelling and slab melting. *Lithos* **121**, 117–134 (2011).
74. Gazel, E. et al. Continental crust generated in oceanic arcs. *Nat. Geosci.* **8**, 321 (2015).
75. Madrigal, P. et al. A melt-focusing zone in the lithospheric mantle preserved in the Santa Elena ophiolite, Costa Rica. *Lithos* **230**, 189–205 (2015).
76. Madrigal, P., Gazel, E., Flores, K. E., Bizimis, M. & Jicha, B. Record of massive upwellings from the Pacific large low shear velocity province. *Nat. Commun.* **7**, 13309 (2016).
77. Li, L. & Bebout, G. E. Carbon and nitrogen geochemistry of sediments in the Central American convergent margin: Insights regarding subduction input fluxes, diagenesis, and paleoproductivity. *J. Geophys. Res. Solid Earth* **110**, B11202 (2005).
78. Holloway, J. R. & Blank, J. G. Application of experimental results to COH species in natural melts. *Rev. Mineral.* **30**, 187–230 (1994).
79. Ohmoto, H. & Rye, R. O. in *Geochemistry of Hydrothermal Ore Deposits* (ed. Barnes, H. L.) 509–567 (1979).
80. de Moor, J. M. et al. Short-period volcanic gas precursors to phreatic eruptions: insights from Poás Volcano, Costa Rica. *Earth Planet. Sci. Lett.* **442**, 218–227 (2016).
81. Kimura, G. et al. (eds) in *Proceedings of the Ocean Drilling Program, Initial Reports Vol. 170 Initial Reports, Costa Rica Accretionary Wedge* (ODP, 1997).
82. Barckhausen, U., Ranero, C. R., Huene, R. V., Cande, S. C. & Roeser, H. A. Revised tectonic boundaries in the Cocos Plate off Costa Rica: implications for the segmentation of the convergent margin and for plate tectonic models. *J. Geophys. Res. Solid Earth* **106**, 19207–19220 (2001).
83. DeMets, C. A new estimate for present day Cocos Caribbean plate motion: Implications for slip along the Central American volcanic arc. *Geophys. Res. Lett.* **28**, 4043–4046 (2001).
84. Patino, L. C., Carr, M. J. & Feigenson, M. D. Local and regional variations in Central American arc lavas controlled by variations in subducted sediment input. *Contrib. Mineral. Petrol.* **138**, 265–283 (2000).
85. Von Huene, R., Langseth, M., Nasu, N. & Okada, H. A summary of Cenozoic tectonic history along the IPOD Japan Trench transect. *Geol. Soc. Am. Bull.* **93**, 829–846 (1982).
86. Parkes, R. J., Cragg, B. A., Fry, J. C., Herbert, R. A. & Wimpenny, J. W. T. Bacterial biomass and activity in deep sediment layers from the Peru margin. *Phil. Trans. R. Soc. Lond. A* **331**, 139–153 (1990).
87. Biddle, J. F. et al. Heterotrophic Archaea dominate sedimentary subsurface ecosystems off Peru. *Proc. Natl Acad. Sci. USA* **103**, 3846–3851 (2006).
88. Vannucchi, P. & Tobin, H. Deformation structures and implications for fluid flow at the Costa Rica convergent margin, ODP Sites 1040 and 1043, Leg 170. *J. Struct. Geol.* **22**, 1087–1103 (2000).
89. Spinelli, G. A. & Underwood, M. B. Character of sediments entering the Costa Rica subduction zone: implications for partitioning of water along the plate interface. *Island Arc* **13**, 432–451 (2004).

90. Ranero, C. R. et al. Hydrogeological system of erosional convergent margins and its influence on tectonics and interplate seismogenesis. *Geochem. Geophys. Geosyst.* **9**, Q03S04 (2008).

91. Spinelli, G. A. & Saffer, D. M. Along-strike variations in underthrust sediment dewatering on the Nicoya margin, Costa Rica related to the updip limit of seismicity. *Geophys. Res. Lett.* **31**, L04613 (2004).

92. Lloyd, K. G. et al. Effects of dissolved sulfide, pH, and temperature on growth and survival of marine hyperthermophilic archaea. *Appl. Environ. Microbiol.* **71**, 6383–6387 (2005).

93. Edgcomb, V. P. et al. Survival and growth of two heterotrophic hydrothermal vent archaea, *Pyrococcus* strain GB-D and *Thermococcus fumicolans*, under low pH and high sulfide concentrations in combination with high temperature and pressure regimes. *Extremophiles* **11**, 329–342 (2007).

94. Marlow, J. J. et al. Carbonate-hosted methanotrophy represents an unrecognized methane sink in the deep sea. *Nat. Commun.* **5**, 5094 (2014).

95. Boetius, A. & Wenzhöfer, F. Seafloor oxygen consumption fuelled by methane from cold seeps. *Nat. Geosci.* **6**, 725 (2013).

96. Hensen, C., Wallmann, K., Schmidt, M., Ranero, C. R. & Suess, E. Fluid expulsion related to mud extrusion off Costa Rica—a window to the subducting slab. *Geology* **32**, 201–204 (2004).

97. Colwell, F. S. et al. Estimates of biogenic methane production rates in deep marine sediments at Hydrate Ridge, Cascadia Margin. *Appl. Environ. Microbiol.* **74**, 3444–3452 (2008).

98. Sánchez-Murillo, R. et al. Geochemical evidence for active tropical serpentinization in the Santa Elena Ophiolite, Costa Rica: an analog of a humid early Earth? Geochem. *Geophys. Geosyst.* **15**, 1783–1800 (2014).

99. Crespo-Medina, M. et al. Insights into environmental controls on microbial communities in a continental serpentinite aquifer using a microcosm-based approach. *Front. Microbiol.* **5**, 604 (2014).
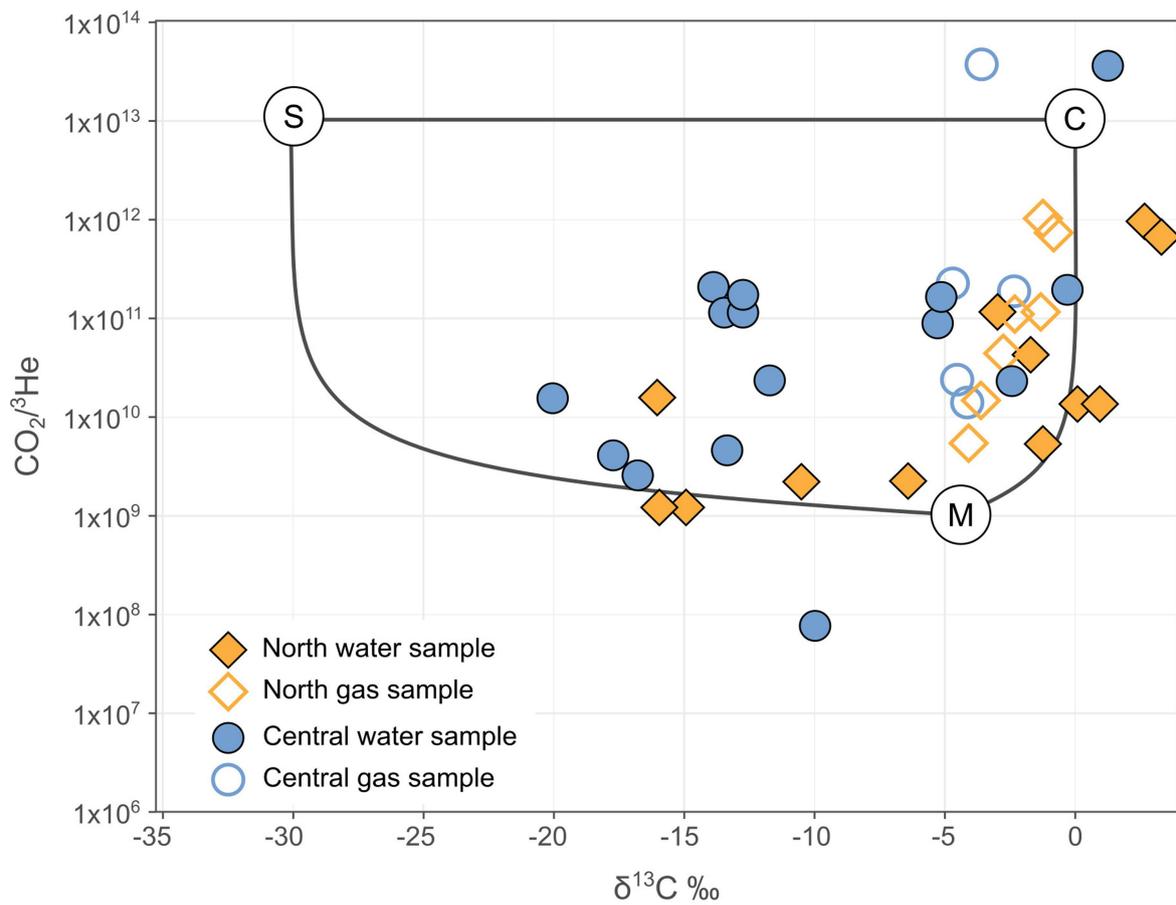
Extended Data Fig. 1 | CO$_2$/^{3}He versus δ^{13}C for all samples collected, together with mixing lines between mantle (M), organic sediment (S) and carbonate (C) endmembers. We argue that such mixing relationships cannot easily explain the water data, and that instead carbon isotope fractionation associated with calcite precipitation and chemolithoautotrophy introduces the observed δ^{13}C variations.
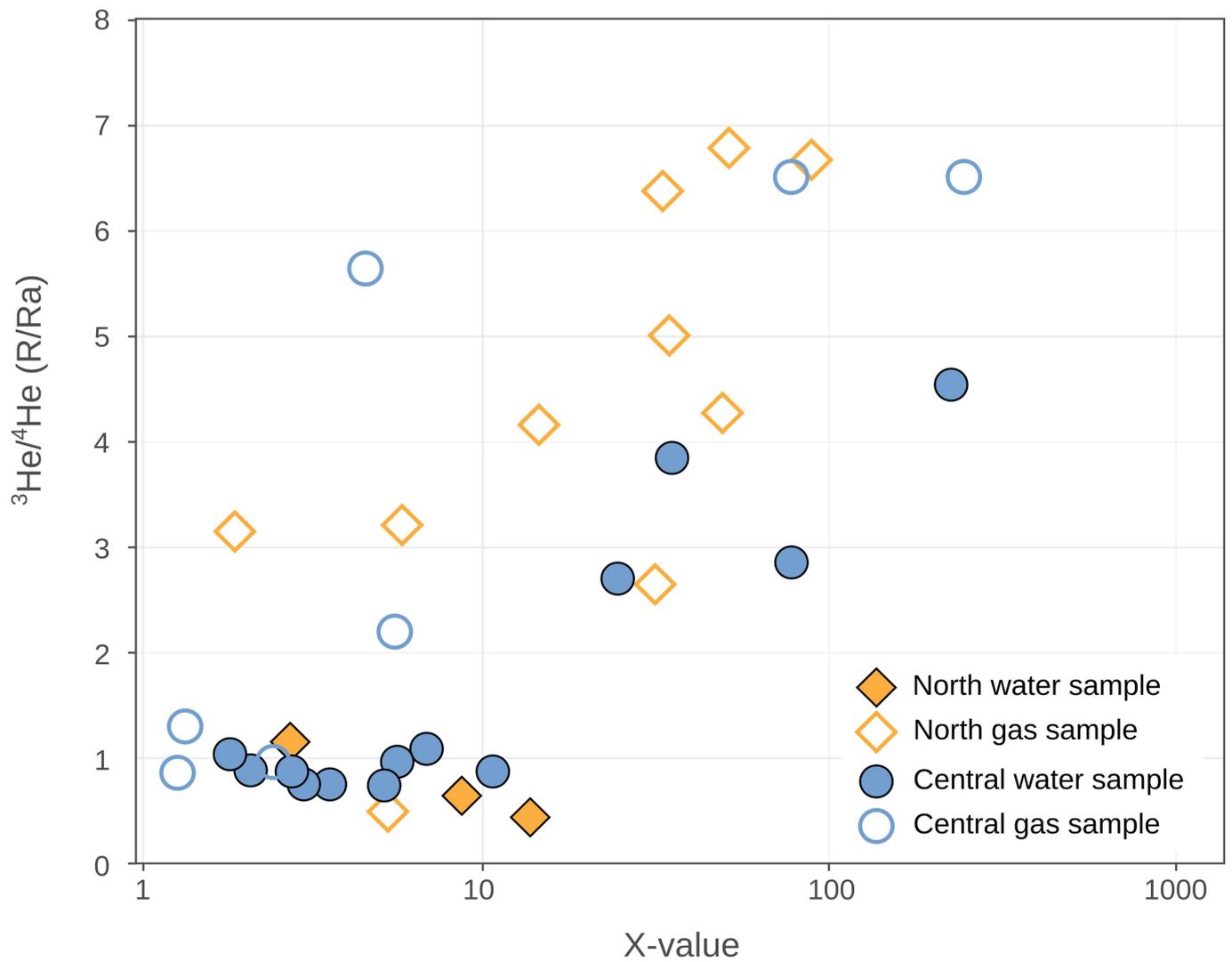
Extended Data Fig. 2 | Helium isotopes (^{3}He/^{4}He) versus X values. The X values are air-normalized ^{4}He/^{20}Ne; considering solubility in water for fluid samples[23]. The majority of samples have high (>5) X values, indicating minimal air-contributions to samples.
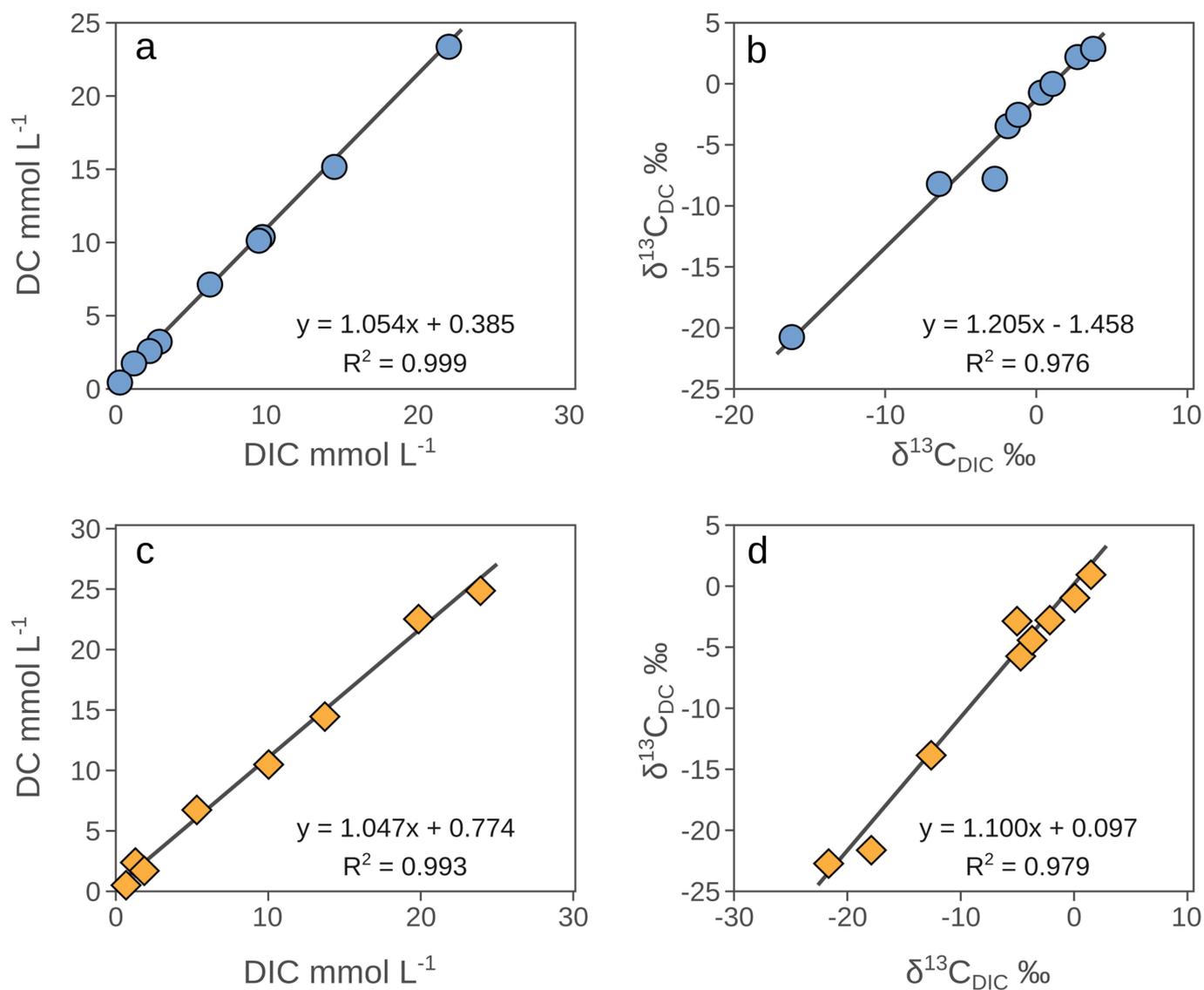
Extended Data Fig. 3 | Relationship between DC and DIC concentrations and δ^{13}C. Values for northern Costa Rica (**a** and **b**) are shown with blue symbols and central Costa Rica (**c** and **d**), with yellow symbols. Strong correlations allow prediction of DC concentrations and δ^{13}C values for the sites for which DIC compositions are lacking. The slope of the concentration plots (*y*) is used to calculate the fraction of DIC and DOC in the sample suites.